Journal of Materials Chemistry A

ROYAL SOCIETY OF CHEMISTRY

PAPER

View Article Online
View Journal

Cite this: DOI: 10.1039/d6ta01756h

Adsorption of conducting polymer to high-surface-area nanoengineered cellulose fibers to facilitate rapid fabrication of highly conductive papers

Nuzhet I. Kilic, †[ab] Johanna Sjölund, †[ac] Yunfan Lin, [def] Marica Muccini, [fgh] Erica Zeglio, [fghij] Tobias Benselfelt, [a] Mahiar M. Hamedi *[ab] and Per A. Larsson *[abc]

Paper is an attractive substrate for sustainable and scalable organic electronics; however, its intrinsically insulating nature, the absence of continuous electronic pathways, and the lack of control over mixed ionic–electronic transport have limited its use in electrochemical devices. Here, we nanoengineer cellulose fibers by introducing cationic charges to facilitate a high specific surface area accessible for the adsorption of functional components. We further speed up the diffusion-controlled adsorption through controlled partial fibrillation of the fibers. The combined cationic charge and high surface area enabled high adsorption of the conducting polymer PEDOT:PSS (poly(3,4-ethylenedioxythiophene):polystyrene sulfonate) throughout the internal nanostructure of the fiber wall. The modified fibers were then rapidly transformed to mechanically robust, electrically conductive papers using a conventional papermaking methodology. Post-treatment of papers containing 30 wt% PEDOT:PSS resulted in excellent charge transport and a conductivity as high as 13 S cm^{-1}. Furthermore, electrochemical impedance spectroscopy of wet papers confirmed effective mixed ionic–electronic transport. Finally, to demonstrate the possibilities of the electroactive paper, we integrated the paper as channel materials in organic electrochemical transistors and evaluated them as enzyme-free hydrogen peroxide sensors, achieving a limit of detection of 0.79 μM and a sensitivity of 8.5% per decade, highlighting the potential of combining fiber-wall engineering with scalable processing and device integration.

Received 27th February 2026
Accepted 26th May 2026

DOI: 10.1039/d6ta01756h

rsc.li/materials-a

1. Introduction

Paper is one of the most widely produced and used materials in the world.[1,2] Traditionally, papermaking has focused on waste reduction, process and material efficiency, and mechanical performance, making paper one of the most recycled materials available.[3–8] These advances have established paper as a mechanically robust and both economically and environmentally attractive substrate. However, from an electrical functionality perspective, conventional cellulose fibers and paper, as encountered in everyday life, completely lack this and serve primarily as an electrical insulator in devices such as transformers.[9,10] But, the raw material for papermaking – cellulose fibers – has an intriguing nanoarchitecture with an untapped scaling potential from a nanoscience point of view. If electrical conductivity could be introduced within each fiber while preserving strength, flexibility, and sustainability, paper could evolve into a multifunctional platform for lightweight, biodegradable, and flexible systems in sensing, energy storage, actuation, and communication.[11]

Current strategies for paper-based electronics rely largely on printing or coating conductive and semiconductive materials onto the paper surface.[11–15] Such surface-localized approaches

[a]Department of Fibre and Polymer Technology, KTH Royal Institute of Technology, Teknikringen 56–58, SE-100 44 Stockholm, Sweden. E-mail: mahiar@kth.se; perl5@kth.se
[b]DCC Digital Cellulose Center, Department of Fibre and Polymer Technology, KTH Royal Institute of Technology, Teknikringen 56–58, SE-100 44 Stockholm, Sweden
[c]FibRe Centre for Lignocellulose-based Thermoplastics, Department of Fibre and Polymer Technology, KTH Royal Institute of Technology, Teknikringen 56–58, SE-100 44 Stockholm, Sweden
[d]Department of Protein Science, SciLifeLab, KTH Royal Institute of Technology, Tomtebodavägen 23a, SE-171 65 Solna, Sweden
[e]Wallenberg Initiative Materials Science for Sustainability, Department of Protein Science, KTH Royal Institute of Technology, Tomtebodavägen 23a, SE-171 65 Solna, Sweden
[f]AIMES – Center for the Advancement of Integrated Medical and Engineering Sciences, Department of Neuroscience, Biomedicum, Karolinska Institutet, Solnavägen 9, SE-171 65 Solna, Sweden
[g]Department of Chemistry, Stockholm University, Svante Arrhenius Väg 16C, SE-114 18 Stockholm, Sweden
[h]Wallenberg Initiative Materials Science for Sustainability, Department of Chemistry, Stockholm University, Svante Arrhenius Väg 16C, SE-114 18 Stockholm, Sweden
[i]Digital Futures, Department of Chemistry, Stockholm University, Svante Arrhenius Väg 16C, SE-114 18 Stockholm, Sweden
[j]Center for Circular and Sustainable Systems (SUCCeSS), Stockholm University, SE-106 91 Stockholm, Sweden
† These authors contributed equally to this work; author order reflects relative contribution.

might, however, suffer from limited adhesion and mechanical durability when bent. They can also be sensitive to humid or wet conditions. Moreover, confining active materials to the surface restricts electrical integration within the fibrous network and might limit both mechanical robustness and charge transport. Lastly, utilization of the paper surface only is an inefficient use of the material. A more effective strategy is to incorporate electroactive components directly within the fiber nanostructure, thereby enabling volumetric electrical integration while retaining compatibility with conventional papermaking.

Cellulose fibers are hierarchical structures based on cellulose nanofibril (CNF) assemblies, offering a large internal surface area that remains largely inaccessible in conventional fibers. Previous efforts have explored CNF-based conductive nanopapers; however, their energy-intensive production and slow dewatering kinetics hinder compatibility with industrial papermaking infrastructure.[16–20] Consequently, fiber-based conductive papers offer a more scalable, cost-effective, and industrially adaptable route toward sustainable electronic materials.

For large-scale production of electroactive paper, efficient retention of electroactive materials during papermaking is required. In our earlier work, we modified cellulose fibers to hold a slight cationic charge ($\sim$300 μeq g^{-1}).[21] These fibers efficiently adsorbed anionic electroactive nanoparticles, including carbon nanotubes and the conductive polymer poly(3,4-ethylenedioxythiophene):polystyrene sulfonate (PEDOT:PSS), enabling the production of electroactive papers using standard papermaking processes.[21] The papers were recyclable, and retained their intrinsic properties. However, adsorption remained largely confined to the external fiber surface, limiting the achievable adsorption to 1 wt% and the concomitant conductivity to 0.028 S cm^{-1} for PEDOT:PSS.[21] Here, we overcome this limitation by increasing the fibre charge ($\sim$1000 μeq g^{-1}) to fully access the interior nanoarchitecture,[22,23] and thereby significantly increasing the electroactive loading.

Among the conductive nanoparticles that can enter and adsorb inside the fiber wall after proper chemical modification, PEDOT:PSS is particularly attractive due to its processability, durability, and intrinsic conductivity.[24] As an organic conductor, it may offer advantages over inorganic counterparts when combined with cellulose, helping to preserve flexibility, minimize interfacial mismatches and enable more sustainable end-of-life pathways compared to inorganic alternatives. Based on these considerations, we demonstrate an industrially scalable process that combines high cationic fiber charge with partial fiber wall fibrillation to maximize the availability of the fiber interior. This enabled up to 30 wt% adsorption of PEDOT:PSS to the modified cellulose fibers. Conductive papers were produced within minutes using laboratory-scale papermaking, and their conductivity could be further enhanced by several orders of magnitude through post-processing, reaching values up to 13 S cm^{-1}. Finally, we demonstrate multifunctionality by employing these papers as the active channel material in organic electrochemical transistors (OECTs). The devices exhibit clear transistor behavior, and efficient charge transport. Using hydrogen peroxide as a model analyte, the OECTs had a limit of detection (LOD) of 0.79 μM and a sensitivity of $\sim$8.5% per decade, highlighting the electroactive paper's potential for scalable bioelectronic applications.

2. Results and discussion

2.1. Cellulose fiber engineering and PEDOT:PSS adsorption

Most electroactive nanomaterials and conductive polymers that are dispersible in water carry a net negative surface charge.[25,26] Effective integration of such materials into cellulose-based systems therefore requires positively charged fiber surfaces. Native cellulose fibers, however, generally carry a weak anionic charge, originating from residual hemicellulose and extractives, as well as oxidized lignin formed during pulping and bleaching processes.[27] To overcome this, we chemically modified conventional cellulose fibers to carry cationic charges by etherification using 3-chloro-2-hydroxypropyltrimethylammonium chloride (details in the Experimental section), resulting in a high cationic charge of approximately 1000 μeq g^{-1}.

Besides enabling electrostatic interaction, high charge induces pronounced fiber wall swelling, substantially increasing the accessibility to the internal nanoarchitecture of each fiber. To put this in numbers, the specific surface area of the external surface of a dry fiber is only $\sim$1 m^2 g^{-1}; upon exposure of nanofibril aggregates, this value increases to $\sim$90 m^2 g^{-1}, and full nanofibril individualized yields $\sim$600 m^2 g^{-1} (see the SI).[23,28] At sufficiently high charge, PEDOT:PSS therefore adsorbs not only on the external fiber surface but also throughout the fiber interior, enabling adsorption of high doses of the nanoparticles (Fig. 1a).

The electrostatic coupling between cationic cellulose fibers and anionic PEDOT:PSS leads to efficient, entropically driven physical adsorption, ensuring robust PEDOT:PSS retention. Because fiber swelling and adsorption capacity are governed by the fibers' total charge, we systematically optimized and quantified the PEDOT:PSS loading relative to the fiber charge. By this we ended up adding PEDOT:PSS to the cationic fiber suspensions at charge ratios of 80% and 160% relative to the fiber's total charge, corresponding to approximately 20 wt% and 30 wt% PEDOT:PSS, respectively. Successful adsorption was observed visually and by Fourier-transform infrared (FT-IR) spectroscopy, which showed indicative bands of both the cationic group and the adsorbed PEDOT:PSS (Fig. S1).[31–33] Furthermore, polyelectrolyte titration of the filtrates using the cationic polyelectrolyte poly(diallyldimethylammonium chloride) showed no detectable residual PEDOT:PSS, indicating complete adsorption of the added polymer (SI, Table S1).

Owing to the nanoscopic dimensions inside the swollen fiber wall, the adsorption onto the interior surfaces is governed by the diffusion of PEDOT:PSS into the fiber wall, making the process strongly time-dependent. To investigate this dependence, we monitored adsorption (20 wt% target loading) over time. After one day, the fibers adsorbed approximately 8 wt% PEDOT:PSS; after four days, adsorption was complete (SI, Table S2 and Fig. 1b). The adsorption values exceed previously reported PEDOT:PSS loadings on cellulose fibers by more than an

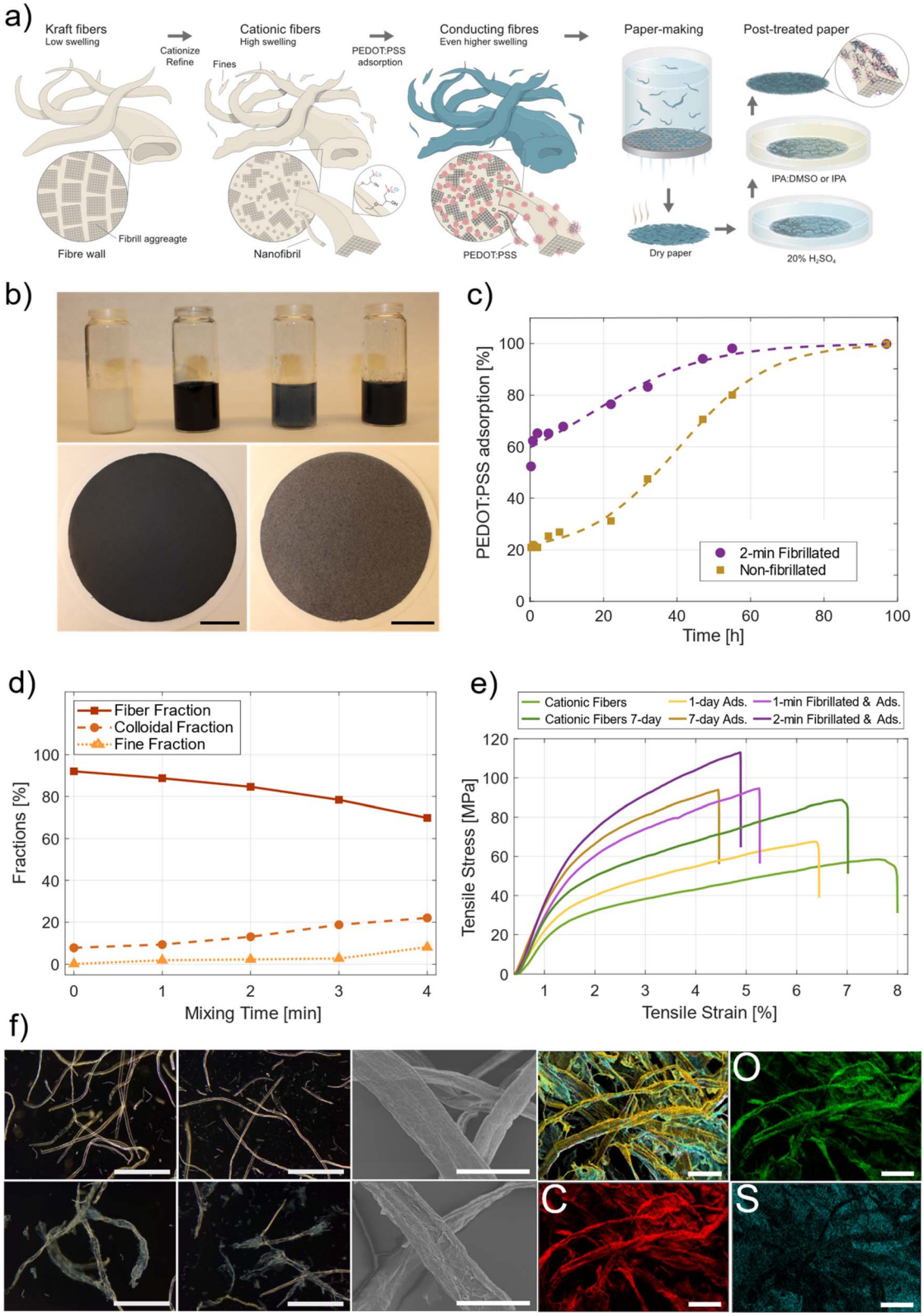

Fig. 1 (a) Schematic illustration of the processing route, starting from cellulose fibers, which were subjected to cationization and blending to enhance fiber wall swelling and accessibility, adsorption of PEDOT:PSS, papermaking, and post-treatment to yield conductive paper. (b) Top: vials (from left to right) containing cationic fibers, PEDOT:PSS stock solution, and samples after one day and seven days of PEDOT:PSS adsorption. Bottom: fabricated papers (from left to right) showing seven-day- and one-day-adsorption samples. (c) Adsorption isotherms; adsorption of PEDOT:PSS onto non-fibrillated and 2 min pre-fibrillated cationic fibers. (d) Fiber, fine, and colloidal fractions of pre-fibrillated samples at different blending times; 0 min corresponds to non-blended cationized fibers. (d) Representative tensile curves of laboratory sheets prepared from cationized fibers, pre-fibrillated cationized fibers, and PEDOT:PSS-adsorbed fibers. (f) Dark-field optical microscopy images: (top,

order of magnitude, where adsorption was limited to 1 wt%.[21] The unprecedented uptake arises from two synergistic effects: (i) the high cationic charge increases the number of binding sites, and (ii) charge-induced osmotic swelling of the fiber wall dramatically increases its accessibility, enabling penetration beyond the external surface. In addition, agitation during adsorption may further promote accessibility by introducing partial fibrillation of the fiber wall, exposing additional internal surfaces.[22,29] Indeed, our reference cationic fiber suspensions subjected to continuous mild stirring developed a gel-like appearance over seven days, indicating pronounced fiber swelling and/or partial fibrillation (Fig. S2).

Long adsorption times may limit scalability. Therefore, to accelerate adsorption, we introduced controlled mechanical pre-fibrillation to increase the fiber accessibility. The fibers were mechanically pre-fibrillated using a blender for 1–4 minutes prior to PEDOT:PSS adsorption, and the adsorption process was monitored by measuring the time required for the cellulose fibers to reach a PEDOT:PSS loading of approximately 20 wt%. Pre-fibrillation treatments of two and four minutes reduced the adsorption time to approximately 50 and 17 hours, respectively.

To better understand the adsorption process, adsorption isotherms were constructed for the non-fibrillated and the two-minute fibrillated samples (Fig. 1c). We observed considerable differences between the two samples at short adsorption times (<1 hour), with the fibrillated sample adsorbing significantly more PEDOT:PSS. After 45 minutes, the adsorbed amounts of PEDOT:PSS to the fibers were 5 wt% and 13 wt% (22% and 62% of the dosed amount) for the non-fibrillated and the two-minute fibrillated samples, respectively. The enhanced initial adsorption indicates an increased accessibility of the binding sites/area for adsorption. Indeed, following pre-fibrillation, the fraction of largely intact fibers decreased from approximately 90 wt% to 70 wt%, while the fraction of colloidal material and fines, with expected higher surface area, increased (Fig. 1d), which explains the observed behavior at short adsorption times. After initial adsorption, the adsorption kinetics followed a sigmoidal adsorption progression, which could successfully be described by a generalized logistic model ($R^2 = 0.997$ and 0.962 for the non-fibrillated and two-minute fibrillated sample, respectively). The initial slow progression, acceleration, and final decline in adsorption rate indicate a diffusion-limited adsorption process, likely linked to PEDOT:PSS penetrating into the fiber wall. A gradual increase in accessibility could account for the enhanced adsorption rates observed before adsorption reaches saturation (when all PEDOT:PSS is adsorbed).

Excessive fibrillation is known to significantly prolong dewatering during papermaking,[30] which was also observed in this work (Table S3). Hence, we selected two minutes of pre-fibrillation as a compromise and applied this in all subsequent experiments. Under these adjusted conditions, PEDOT:PSS adsorption reached completion within approximately 50 hours, while laboratory handsheets dewatered within two minutes (Table S3). Although conventional fibers dewater within seconds (~10 s), the observed time remains practical at the laboratory scale, and reflects a balance between efficient adsorption and processability. This optimized pre-fibrillation and adsorption sequence enabled direct fabrication of highly conductive, fully organic papers.

2.2. Structure–property relationships in PEDOT:PSS-containing papers

Consistent with the observation of a lower fraction of intact fibers (Fig. 1d), dark-field optical microscopy visually revealed partial fibrillation following pre-fibrillation (Fig. 1f). Following PEDOT:PSS adsorption, additional swelling and partial fiber wall delamination can be observed. The observable difference in swelling between both non-fibrillated and fibrillated fibers and their PEDOT:PSS-adsorbed counterparts is a clear indication that PEDOT:PSS penetrates into the fiber wall rather than adsorbing onto the external surface of the fiber, in accordance with theoretical considerations and observed adsorption kinetics (Fig. 1c). Furthermore, the results suggest that the polymer adsorption itself may act to increase the fiber wall accessibility, possibly explaining the accelerated adsorption rates observed at long adsorption times. This enhanced accessibility from the adsorption likely aids penetration of PEDOT:PSS into the fiber wall as the adsorption progresses. Scanning electron microscopy (SEM) further supports this structural evolution at the individual fiber level, revealing greater fiber wall swelling and more extensive fibrillation (Fig. 1f). Under a SEM, we also evaluated the elemental distribution of PEDOT:PSS in the fibers using energy-dispersive X-ray (EDX) analysis (Fig. 1f). EDX detected sulfur, a characteristic element of PEDOT:PSS absent in cellulose, along the fiber contours, supporting continuous polymer presence along the fibers. Together, FT-IR spectroscopy, adsorption isotherms, titration, and microscopy imaging confirm successful incorporation of PEDOT:PSS within the cationic cellulose fibers.

Mechanical robustness of a material is essential for many applications. Since both PEDOT:PSS adsorption and partial fiber fibrillation are expected to strongly influence the mechanical performance of the papers fabricated, we performed tensile testing (Fig. 1e and Table S4). Pre-fibrillation significantly increased both the elastic modulus and the tensile strength of the papers prepared from cationic fibers. This response parallels conventional papermaking, where mechanical treatment (referred to as beating) induces partial fibrillation, increasing the fiber–fiber contact area and sheet density, which consequently improves stiffness and strength. Consistent with our earlier findings that cationization alone

left to right) cationized and pre-fibrillated cationized fibers; (bottom, left to right) cationized and pre-fibrillated PEDOT:PSS-adsorbed samples. Scale bars: 1 mm; SEM images of (top) cationized fibers and (bottom) pre-fibrillated and PEDOT:PSS-adsorbed samples. Scale bars: 50 μm; layered EDX images of the pre-fibrillated and PEDOT:PSS-adsorbed samples; K_α emission maps corresponding to carbon, oxygen, and sulfur. Scale bars: 100 μm.

improves mechanical performance of the paper,[31] further strength improvements could be observed following partial fibrillation of the fibers prior to papermaking. Among all samples, papers prepared from pre-fibrillated, PEDOT:PSS-adsorbed fibers exhibited the highest elastic modulus and tensile strength. The observed improvement in mechanical properties correlates with an observed increased paper density (Table S4), which likely arises from improved conformability of the swollen fiber network and the presence of PEDOT:PSS within the structure. In addition, the increased fines content further contributes by increasing the bonded area and joint density within the sheet, promoting densification. The observed improvements in stiffness and strength of sheets prepared from PEDOT:PSS-adsorbed fibers were accompanied by a modest reduction in strain-at-break. This decrease may reflect a restricted fiber mobility upon PEDOT:PSS adsorption; with increasing polymer content, the strain approaches that of pure PEDOT:PSS films (2%).[34]

2.3. Electrical conductivity and post-treatment effects

After ensuring good mechanical properties of the papers fabricated, we measured their in-plane electrical conductivity using a two-probe configuration. Papers containing 20 wt% PEDOT:PSS exhibited a conductivity of 0.60 ± 0.03 S cm^{-1}, while increasing the loading to 30 wt% raised the conductivity to 0.9 ± 0.1 S cm^{-1} (Fig. 2a), representing more than a 30-fold improvement over the 0.028 S cm^{-1} reported in our earlier work at 1 wt% loading.[21] These values are on par with or even surpass those of untreated pristine PEDOT:PSS films (~0.50 S cm^{-1}).[35] To further boost charge transport, we applied an acid-solvent post-treatment (see the Experimental section). The post-treatment increased the conductivity by more than one order

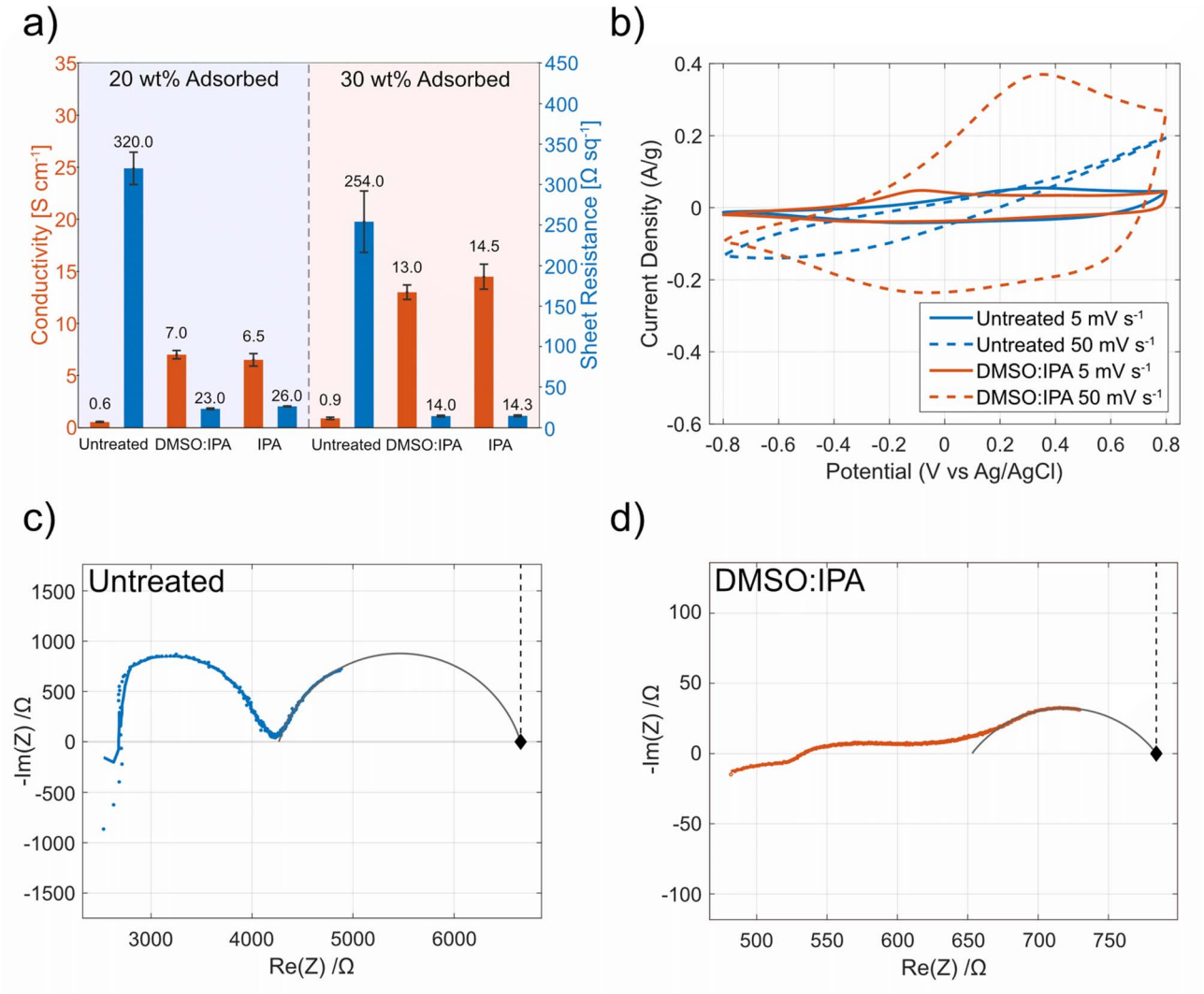

Fig. 2 (a) Electrical conductivity and sheet resistance of pre-fibrillated and PEDOT:PSS-adsorbed samples, before and after post-treatment by acid dipping, followed by treatment with either a DMSO:IPA mixture or IPA alone. (b) CV curves of pre-fibrillated and 20 wt% PEDOT:PSS papers with and without DMSO:IPA treatment, recorded at scan rates of 5 and 50 mV s^{-1}. In-plane Nyquist plots of (c) untreated and (d) acid- and DMSO:IPA-treated 20 wt% PEDOT:PSS papers obtained by EIS. Dashed lines mark the low-frequency real-axis intercept from graphical semi-circle evaluation, representing the electronic conduction contribution.

of magnitude (Fig. 2a): the conductivity of papers containing 20 wt% PEDOT:PSS increased from 0.60 ± 0.03 to 7.0 ± 0.4 S cm^{-1}, while that of papers with 30 wt% PEDOT:PSS increased from 0.9 ± 0.1 to 13.0 ± 0.7 S cm^{-1}. This enhancement is consistent with earlier-observed solvent-induced structural rearrangement in PEDOT:PSS systems, which improves interdomain connectivity and reduces the insulating contribution of PSS.[36,37] As expected, the acid treatment reduced the mechanical strength of the papers (Table S4). This decrease in mechanical performance is consistent with acid-catalyzed hydrolysis of cellulose reported in previous studies, where acidic conditions promote cleavage of glycosidic bonds within the cellulose chains, leading to a reduction in the degree of polymerization.[38,39] Shortening of the cellulose chains weakens the fiber structure and consequently reduces the mechanical strength of the resulting paper network. We found that subsequent dimethyl sulfoxide:isopropyl alcohol (DMSO:IPA) treatment mitigated this degradation and partially restored mechanical performance compared to IPA-only treatment. On this basis, we selected the DMSO:IPA-treated papers for subsequent analysis, as they provide the most favorable balance between electrical conductivity and mechanical integrity.

Under the fabrication conditions selected as a suitable balance between mechanical and electrical properties, the resulting papers achieved sheet resistances of 23 ± 1 Ω sq^{-1} (20 wt%) and 14 ± 1 Ω sq^{-1} (30 wt%), corresponding to electrical conductivities of 7.0 ± 0.4 S cm^{-1} and 13.0 ± 0.7 S cm^{-1}, respectively (Fig. 2a). A quantitative comparison with representative PEDOT:PSS-based conductive paper systems from the literature is summarized in Table S5. Vapor-phase-polymerized papers typically exhibit sheet resistances of approximately 30 Ω sq^{-1}.[40] Composite systems based on cationic fibers/PEDOT:PSS/carbon black reach conductivities slightly above ~4 S cm^{-1}.[41] Similarly, cellulose nanofiber/PEDOT:PSS composites with 38.6 wt% loading achieve conductivities of 3.6 S cm^{-1} after post-treatment.[42] In comparison, the conductive papers developed in this work reach conductivities of up to 13.0 S cm^{-1} while maintaining relatively moderate PEDOT:PSS loadings (20–30 wt%), demonstrating competitive or improved electrical performance compared to previously reported conductive paper systems.

To further highlight the advantage of adsorbing PEDOT:PSS inside modified fibers, commercial Whatman paper and cationically modified cellulose paper were, for comparison, dip-coated with PEDOT:PSS and subjected to identical post-treatment conditions, using one-minute-long dip-coating cycles with either one or five cycles (Fig. S3). The coatings appeared non-uniform on both substrates, particularly on Whatman paper. Although the cationically modified paper exhibited stronger coloration, indicating increased polymer uptake, the coating remained heterogeneous and structural degradation occurred during immersion, likely due to excessive swelling. These results highlight the effectiveness of the cationic fiber adsorption strategy in enabling efficient polymer incorporation and high electrical conductivity without relying on complex composite formulations or post-treatment steps.

2.4. Electrochemical transport behavior

Building on the observed structural and electrical enhancements, we next examined the electrochemical properties of the papers to elucidate their ionic and electronic transport behavior. We characterized post-treated and non-treated papers containing 20 wt% PEDOT:PSS by cyclic voltammetry (CV), to assess the coupling between ionic and electronic transport. Both papers exhibit similar electrochemical behavior at lower scan rates (≤10 mV s^{-1}). However, at higher scan rates (≥50 mV s^{-1}), the post-treated paper maintains higher current densities and more distinct redox features (Fig. 2b and S4), indicating improved charge-transport kinetics.

While the more pronounced redox peaks in the post-treated paper suggest a stronger faradaic contribution, the accompanying increase in current response indicates an enhanced electrochemical activity rather than restricted ion transport (Fig. 2b). Together, these features reflect more efficient coupling between ionic and electronic conduction in the post-treated material.

Materials exhibiting mixed ionic-electronic transport are particularly relevant for electrochemically gated systems that rely on volumetric charging and dedoping processes to modulate conductivity. In this context, the post-treated paper is expected to exhibit stronger conductivity modulation under an applied gate bias, potentially translating into higher transconductance in device configurations such as OECTs. At the same time, the appearance of distinct redox peaks suggests that charge exchange could become more localized, potentially limiting the uniformity of volumetric modulation throughout the paper.

Following the electrochemical behavior observed by CV, we next employed electrochemical impedance spectroscopy (EIS) to further elucidate the wet ionic and electronic transport properties of the papers. EIS measurements were performed on post-treated and non-treated papers with 20 wt% PEDOT:PSS adsorption. An in-plane configuration was used to probe lateral charge transport under electrolyte exposure, providing a device-relevant geometry that closely resembles conditions encountered in OECT operation (Fig. 2c and d). The resulting Nyquist plots reveal an enhanced electronic conduction in the post-treated paper, reflected by changes in the second semicircle in the low-frequency region and its intercept with the real axis[19,43–45] (as evidenced by the reduced real-axis intercept corresponding to electronic resistance).

To extract quantitative conductivities from the Nyquist plots, we fitted the low-frequency arc using graphical semicircle fitting and defined the real-axis intercept as the electronic resistance. Using the real-axis intercepts (dashed lines in Fig. 2c and d), we calculated wet electronic conductivities of 1.24 ± 0.02 S cm^{-1} for post-treated samples and 0.098 ± 0.002 S cm^{-1} for non-treated counterparts. The high-frequency intercept of the first semicircle reflects a mixed conduction contribution. The reduced resistance observed for the post-treated samples indicates improved overall transport relative to non-treated papers. The enhanced conductivity and mixed transport following solvent post-treatment are consistent with previous reports of

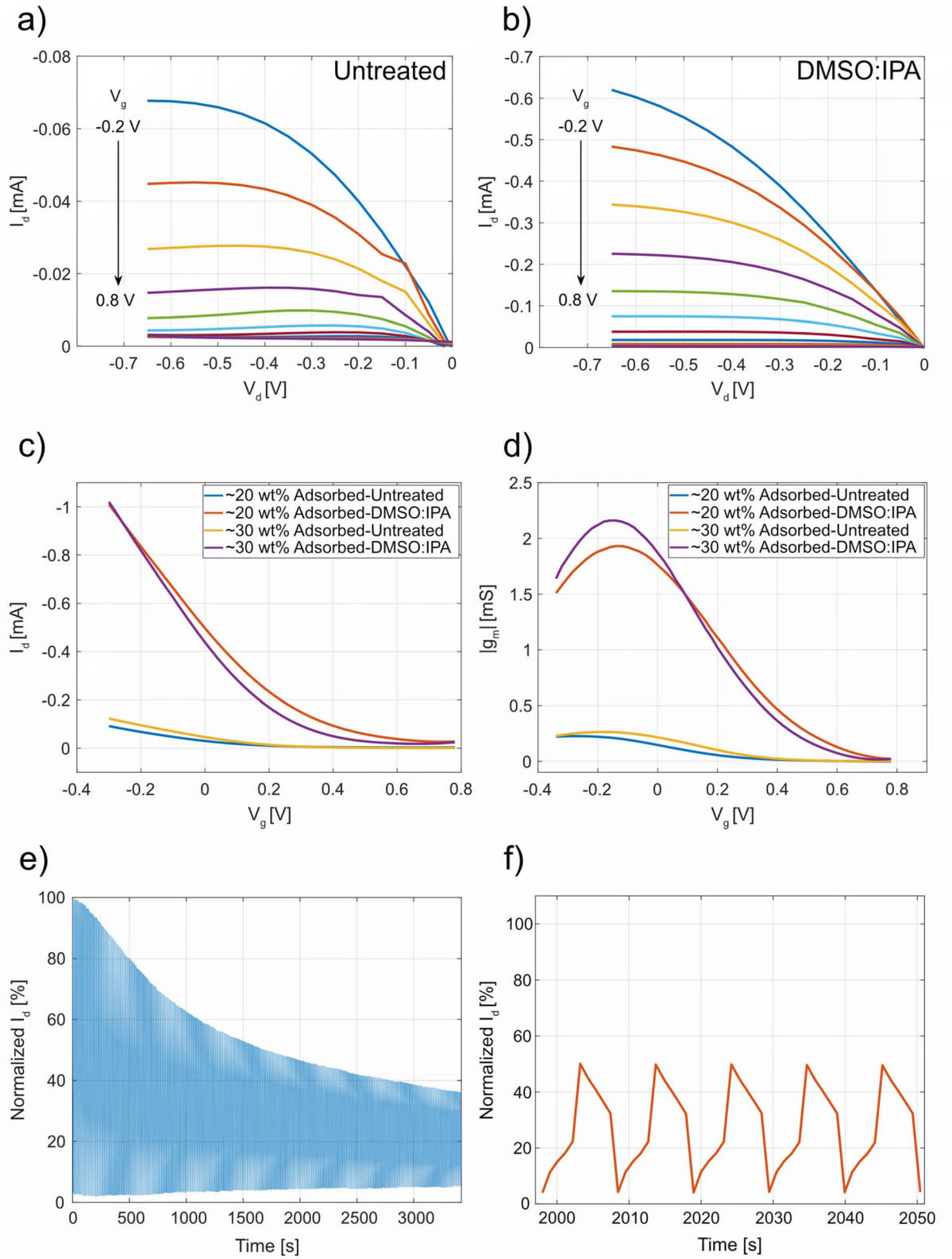

Fig. 3 Output characteristics of representative 20 wt% PEDOT:PSS papers, (a) untreated and (b) post-treated. (c) Transfer behavior and (d) transconductance of representative OECT devices. (e) ON/OFF stability at around 1 h. (f) Normalized drain current *versus* time during five consecutive ON/OFF cycles, starting at $t = 2000$ s.

solvent-induced structural reorganization in PEDOT:PSS systems.[36,46–48] These structural changes likely promote more efficient electronic percolation while maintaining ion accessibility within the porous network.

2.5. OECT characterization

Building upon the electrochemical findings, we integrated the conductive papers as active channels in OECTs to evaluate their transport properties within a device architecture. The porous fiber structure facilitates ion diffusion and volumetric doping of PEDOT:PSS, enabling effective channel modulation. The improved conductivity and transport balance identified by EIS position these materials as suitable platforms for OECT fabrication.

The output characteristics of our electroactive papers exhibit a clear pinch-off behavior at higher drain voltages under increasing gate bias (Fig. 3a, b and S5). Pinch-off arises when the region near the drain undergoes electrochemical dedoping, reducing the charge carrier density and leading to current saturation. The pronounced gate-dependent modulation observed in the output curves aligns with the transfer characteristics (Fig. 3c) and the extracted transconductance (g_m) values (Fig. 3d and e), confirming efficient electrochemical control of the channel. The devices operate in a typical p-type depletion mode, where the drain current (I_d) decreased with increasing gate voltage (V_g), consistent with previously reported PEDOT:PSS-based OECTs.[49,50]

Quantitatively, the $|I_d|$ of the DMSO:IPA-treated papers containing approximately 30 wt% PEDOT:PSS decreased from 1.3 ± 0.3 mA to 0.006 ± 0.003 mA upon gate biasing, corresponding to an I_{ON}/I_{OFF} ratio of about 200. Similarly, the 20 wt% PEDOT:PSS post-treated papers exhibited a decrease from 1.4 ± 0.3 mA to 0.007 ± 0.002 mA, yielding a comparable switching ratio. These results demonstrate efficient channel modulation and a clear turn-off behavior.

The post-treated samples with ~20 wt% and ~30 wt% PEDOT:PSS exhibited the highest I_d levels, consistent with their enhanced conductivity. Both compositions showed maximum $|g_m|$ values of approximately 2.2 mS (2.1 ± 0.2 mS and 2.2 ± 0.3 mS for 20% and 30% PEDOT:PSS, respectively). Notably, the ~30 wt% post-treated devices exhibited transconductance values approximately one order of magnitude higher than those of the corresponding non-treated samples (0.2–0.3 mS), highlighting the impact of solvent post-treatment on device performance. High transconductance reflects efficient current modulation under gate bias and is critical for sensitive OECT-based sensing applications.[51]

Although the extracted transconductance values (~2.2 mS) are lower than those reported in some high-performance OECT studies (up to 21.4 mS),[52] this difference primarily arises from variations in channel geometry and device architecture. The present devices were fabricated using a cleanroom-free, CO_2-laser-defined approach, resulting in larger macroscopic channel dimensions. Because OECT transconductance scales strongly with channel geometry,[53] the observed values are consistent with the geometry and porous nature of the paper-based channels investigated here. Importantly, the fiber-integrated PEDOT:PSS architecture offers advantages in scalability, mechanical robustness, and processing simplicity that conventional microfabricated devices do not. Since the post-treated papers containing ~20 wt% and ~30 wt% PEDOT:PSS exhibited comparable OECT performance, electrical conductivity, and mechanical stability, we selected the ~20 wt% post-treated paper for subsequent hydrogen peroxide sensing experiments.

The long-term behavior was assessed by remeasuring a representative device after approximately six months of storage (Fig. S5). The transfer characteristics show a drain current of approximately 0.6 mA, compared to the initial ensemble average of 1.4 ± 0.3 mA, corresponding to roughly 40–45% of the initial current remaining. Despite this decrease, the device continues to exhibit clear transistor characteristics, which, for the device functionality, is more important than the exact current. The conductive polymer incorporation is consistent with electrostatic interactions between the quaternary ammonium groups of the cellulose fibers and the negatively charged sulfonate groups (PSS^-) of PEDOT:PSS. These interactions anchor the conductive polymer to the fiber surface and reduce the likelihood of polymer detachment during aqueous operation. Consequently, the observed decrease in current over time is more likely associated with gradual changes in the PEDOT:PSS structure or doping state rather than loss of the conductive polymer from the fibers.

To evaluate device behavior under aqueous operating conditions, repeated ON/OFF switching experiments were performed under electrolyte gating for approximately one hour (Fig. 3e and f). During this experiment the PEDOT:PSS channel undergoes repeated electrochemical doping and dedoping cycles. Over the course of continuous operation, the normalized drain current gradually decreases and approaches approximately 40% of its initial value, reflecting the dynamic response of the channel during electrochemical cycling in electrolyte.

2.6. Enzyme-free hydrogen peroxide sensing

To demonstrate sensing capability, we fabricated a hydrogen peroxide sensor using the same channel geometry employed for OECT characterization. A gold disk served as the gate electrode and was sequentially modified by first coating it with PEDOT:PSS to match the electronic and interfacial properties of the channel, thereby promoting consistent mixed transport behavior (Fig. 4a and b).[54] Platinum was subsequently electrodeposited onto the PEDOT:PSS-coated gate to introduce catalytic functionality for hydrogen peroxide reduction.[55,56] CV confirmed successful PEDOT:PSS coating and platinum electrodeposition (Fig. 4b).

We evaluated the sensor response in 10 mM phosphate-buffered saline (PBS) using amperometric measurements across a hydrogen peroxide concentration range of 0.05–1000 μM, spanning the micromolar to sub-millimolar regime relevant for biological and environmental samples.[57] Each concentration was tested using at least three independent devices (Fig. 4c). Following stabilization under bias (see the

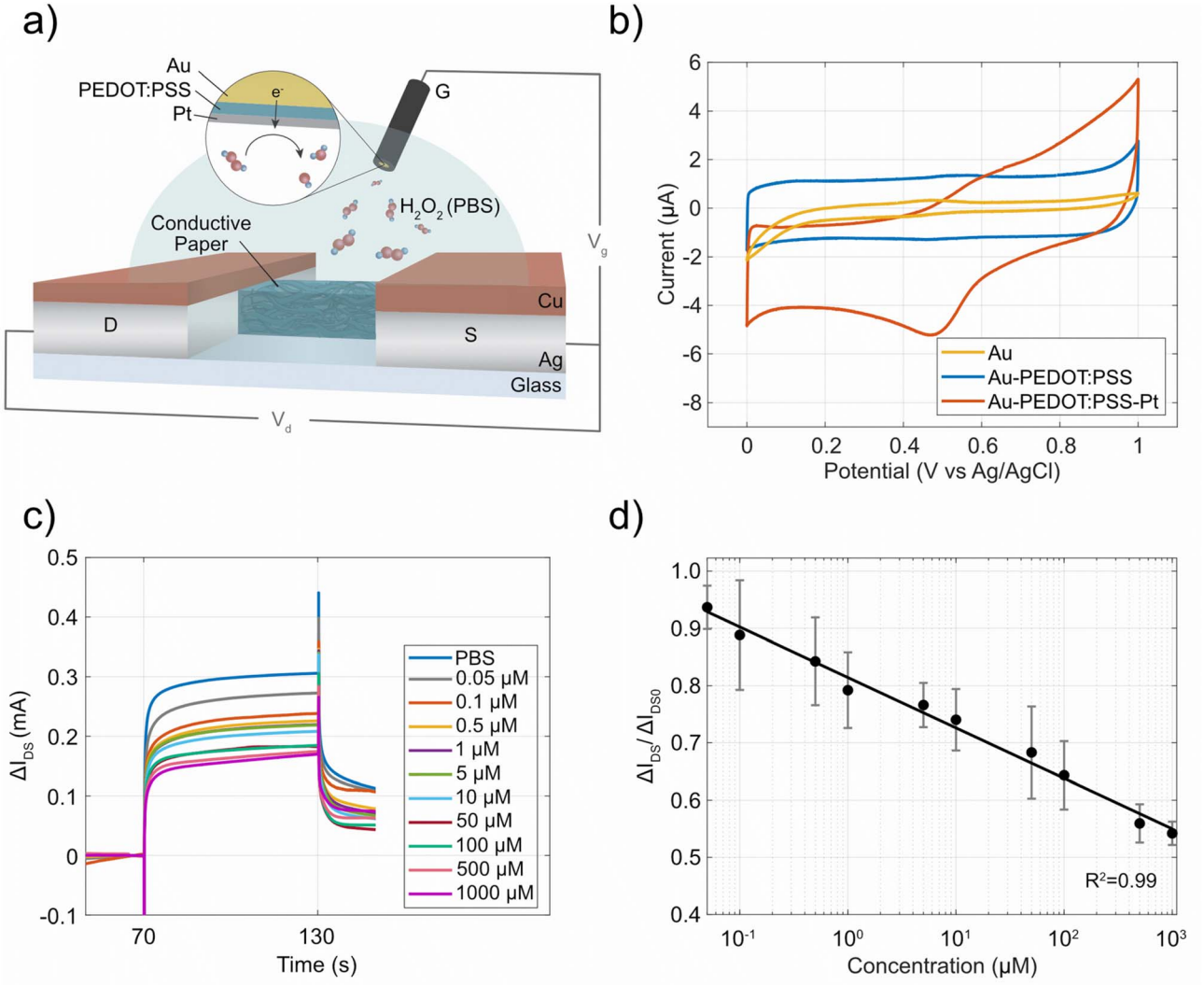

Fig. 4 (a) Schematic illustration of the hydrogen peroxide OECT sensor platform with a PEDOT:PSS-adsorbed paper channel and a modified Au/PEDOT:PSS/Pt gate electrode. (b) CV profiles recorded at 20 mV s^{-1} for bare gold, PEDOT:PSS-coated gold, and PEDOT:PSS-coated gold with electrodeposited platinum. (c) Drain-source current variation over time at different hydrogen peroxide concentrations and 0.8 V gate voltage. (d) Normalized drain-source current changes relative to PBS across varying analyte concentrations.

Experimental section), we applied stepwise gate potentials corresponding to the maximum transconductance identified during device characterization (Fig. S6). Baseline-corrected current–time transients were analyzed relative to each device's current $V_g = 0$ V. Distinct concentration-dependent responses were observed, with increasing hydrogen peroxide concentration leading to a decrease in ΔI_{DS} (Fig. 4c). This response originates from electrochemical reduction of hydrogen peroxide at the platinum-modified gate, which alters the gate potential and modulates the oxidation state of the PEDOT:PSS channel.[54,58] As the analyte concentration increases, partial dedoping of the p-type channel reduces the charge carrier density, resulting in decreased drain current.[54] This mechanism reflects the characteristic signal transduction of p-type OECT sensors, where a gate-side electrochemical reaction is translated into channel current modulation.

Steady-state drain current values extracted from the amperometric traces were used to construct a calibration curve based on the normalized current response ($\Delta I_{DS}/\Delta I_{DS0}$), where ΔI_{DS} denotes the change in drain current measured at different analyte concentrations following gate potential application. ΔI_{DS0} represents the corresponding current change obtained in the electrolyte without any analyte (10 mM PBS) under identical biasing conditions.[59] The data follow a log-linear relationship, described by using:

$$y = -0.0854 \log_{10}(C) + 0.7978 \quad (1)$$

where y represents the normalized response and C is the hydrogen peroxide concentration. As shown in Fig. 4d, the device exhibits a log-linear dependence of the normalized drain current ($\Delta I_{DS}/\Delta I_{DS0}$) on analyte concentration, with a sensitivity of 8.5% per decade, corresponding to an approximately 8.5% change in the normalized current for each tenfold increase in concentration.[60] To further evaluate the sensing performance, the limit of detection (LOD) was estimated using the 3σ

criterion (see the Materials and methods section for details).[61] Using this approach, the LOD of the hydrogen peroxide sensor was estimated to be approximately 0.79 μM.

The paper-based architecture and enzyme-free configuration enable direct electrochemical sensing without biochemical amplification steps while maintaining a measurable response across the investigated concentration range. Together with the electrical and operational characterization presented above, these results define the analytical performance of the fiber-integrated, enzyme-free OECT platform under physiologically relevant conditions.

3. Conclusions

This work demonstrates the effectiveness of combining engineered cellulose fibers with electroactive materials to fabricate highly conductive paper, establishing a versatile platform for advanced organic electronic applications.

By engineering cellulose fibers to exhibit high cationic charge density, we gained access to their internal nanostructure. The exceptional accessibility of the fiber structure, together with electrostatic interactions between cationic cellulose and negatively charged PEDOT:PSS, enabled adsorption levels of up to 30 wt%. This high loading facilitated the production of highly conductive papers *via* conventional papermaking, yielding conductivities that exceed those of previously reported fiber-based systems.

A subsequent post-treatment further enhanced electronic transport, reaching conductivities up to 13 S cm^{-1} for sheets containing 30 wt% PEDOT:PSS. Electrochemical impedance analysis confirmed improved wet transport behavior, indicating more efficient mixed ionic–electronic conduction within the hydrated fiber network.

To demonstrate device applicability, we integrated these electroactive papers as channels in organic electrochemical transistors. The OECTs exhibited stable operation and were further employed as enzyme-free hydrogen peroxide sensors. The devices showed a concentration-dependent response with a limit of detection of 0.79 μM and a sensitivity of 8.5% per decade, confirming effective electrochemical signal transduction without enzymatic amplification.

Together, these findings establish conductive cellulose paper as a scalable, mechanically robust, and multifunctional platform for OECTs and enzyme-free electrochemical sensing, advancing sustainable bioelectronic and organic electronic technologies.

4. Materials and methods

4.1. Materials

Never-dried, fully bleached, softwood Kraft pulp (50 : 50 Scots pine and Norwegian spruce) was obtained from Stora Enso AB, Skoghall mill, Karlstad, Sweden. 3-Chloro-2-hydroxypropyl trimethylammonium chloride solution (CHPTAC, 60.0%), hydrochloric acid (HCl, 37.0%), sodium hydroxide (NaOH, ACS reagent, ≥97.0%), silver nitrate (ReagentPlus®, ≥99.0%), 4-dodecylbenzenesulfonic acid (DBSA, mixture of isomers, ≥95%), ethylene glycol, dimethyl sulfoxide (DMSO, ACS reagent, ≥99.9%), (3-Glycidyloxypropyl)trimethoxysilane (GOPS, ≥98.0%), chloroplatinic acid hexahydrate ($H_2PtCl_2 \cdot 6H_2O$, ACS reagent, ≥37.50% Pt basis), and sulfuric acid (H_2SO_4, ACS reagent, 95.0–98.0%) were purchased from Sigma Aldrich, Sweden. PEDOT:PSS Clevios PH 1000 (PEDOT:PSS, 1.0–1.3 wt%) was obtained from Heraeus Epurio GmbH, Germany. PBS tablets were purchased from Thermofisher Scientific, Sweden. Silver paste used for contacts in the conductivity measurements was purchased from Ladd Research (Conducting Silver Paint, Catalog No. 60805, sheet resistance <0.1 Ω sq^{-1}). Solvents such as 2-propanol and ethanol were of analytical grade and obtained from VWR, Sweden.

4.2. Cationization of cellulose fibers

Prior to use, the fibers were washed to remove contaminants such as metal ions and dissolved colloidal substances.[22] Fiber cationization was carried out on 30 g (dry basis) fiber batches according to the procedure reported previously.[31] For clarification, the hand-mixing and water-bath heating method was used; alkali was dosed at a 1.2 NaOH : reagent ratio, and the reagent (CHPTAC) was dosed at a 2 : 1 reagent:cellulose anhydroglucose unit ratio. The reaction was performed for four hours at 60 °C. The fiber charge was determined using conductometric titration.[31]

4.3. Pre-fibrillation of cationized fibers

Cationized fibers were suspended in 200 mL of DI water to 1 wt%. Mechanical pre-fibrillation was carried out by blending the suspension using a Blendtec Total Blender (1.8 L, 1560 W; Blendtec, Orem, UT, USA) for 1–4 min. The blender was operated at the maximum speed setting.

4.4. PEDOT:PSS adsorption

Following chemical modification and, when applicable, mechanical prefibrillation (0–4 min), fiber suspensions were prepared at a 1 wt% consistency with a total volume of 200 mL and mixed for several minutes using a magnetic stirrer to ensure homogeneous suspension. Prior to addition, the PEDOT:PSS dispersion was homogenized using an Ultra-Turrax at 5000 rpm for 5 min. An amount of PEDOT:PSS corresponding to 80% and 160% charge saturation was then added to the fiber suspension and mixed until partial or full adsorption occurred. The amount of PEDOT:PSS adsorbed onto the fibers was determined indirectly by measuring the amount of non-adsorbed, negatively charged PEDOT:PSS remaining in the filtrate. After adsorption, the fibers were filtered, washed with DI water, and resuspended in water to obtain a final fiber concentration of 1 wt%.

4.5. Paper making

The fiber-PEDOT:PSS suspensions were used for preparations of sheets using a Rapid Köthen paper-making instrument (Paper Testing Instruments, Austria). Suspensions, with a dry fiber content of two grams, were used to obtain sheets with a target

grammage of ~70 g m^{-2}. The fibers, PEDOT:PSS-adsorbed or not, were suspended in 1 L of DI water before being formed into paper sheets. The instrument was operated in manual mode, and the duration of each step is provided in Table S3. The sheets were dried for 15 minutes at 93 °C under a reduced pressure of 95 kPa.

4.6. Post-treatment

Following PEDOT:PSS adsorption and papermaking, some of the material was subjected to post-treatment to further enhance the papers' conductivity. These papers were dipped in a 20 vol% concentrated sulfuric acid solution (in water) for 15 seconds. After blot-drying between filter papers, they were immediately immersed in either pure IPA or an 80 vol% DMSO/IPA mixture for 30 seconds. The treated papers were then dried under a reduced pressure of 95 kPa at 97 °C for 30 minutes, followed by drying in a conventional oven at 60 °C for one hour.

4.7. Characterization techniques

The amount of PEDOT:PSS adsorbed onto the fibers was determined indirectly by establishing the concentration of residual, negatively charged, PEDOT:PSS in the filtrate. This was achieved using a ParticleMetrix Stabino system (ParticleMetrix GmbH, Munich, Germany) with polydiallyldimethylammonium chloride with a known concentration as the counterion titrant. In the case of complete adsorption, no PEDOT:PSS was present in the filtrate and the streaming potential of the filtrate was close to zero. Triplicates were taken for each sample and the average values were reported. Adsorption isotherms were constructed by taking representative fractions of the sample at various stages of the adsorption process and performing the same washing and titration procedure to determine the amount of adsorbed PEDOT:PSS at each time point. Adsorption kinetics at $t \geq 15$ min were analyzed using a generalized logistic sigmoidal model to describe the adsorption progression as a function of time in MATLAB (MathWorks, USA). The upper asymptote was fixed to 100%, corresponding to the equilibrium adsorption capacity.

The fractional composition of the cationized material after blending was determined by fine content and nanoyield measurements. Fines determinations were performed using a Britt Dynamic Drainage Jar (BDDJ); Paper Research Materials (Seattle, WA, USA), equipped with a P125 screen (76 μm hole diameter), which was used following a previously reported procedure.[31] Measurements were performed in duplicate. To determine the colloidally stable fraction, a separate sample was taken from the cationic, blended, fibers corresponding to 0.1 g dry material, and the sample was diluted to 1 g L^{-1} and thoroughly suspended by Ultra-Turrax mixing at 5000 rpm for 5 min followed by centrifugation at 2600*g* for 30 min. The colloidally stable fraction was separated from the fiber/fine fraction by decantation and the fractions were dried separately (105 °C over-night); the fractional composition was measured gravimetrically. Measurements were performed in triplicate.

Dark-field phase-contrast imaging was performed on fibers dispersed in deionized water using a DM IL inverted microscope (Leica, Wetzlar, Germany) equipped with a DMC2900 camera. A diluted fiber suspension was deposited onto a glass microscope slide, covered with a cover slip, and subsequently imaged.

The morphology of dried fibers was examined using a Hitachi S-4800 scanning electron microscope (FE-SEM, Hitachi, Chiyoda, Japan) operated at an accelerating voltage of 5.0 kV. Fibers dispersed in water were first solvent-exchanged to acetone, air-dried at the bench, and mounted on aluminum stubs using conductive carbon tape. Prior to imaging, non-conductive samples were sputter-coated with a 2.2 nm Pd/Pt layer using a 208HR Cressington sputter coater to minimize charging effects. Energy-dispersive X-ray (EDX) analysis and elemental mapping were conducted by using an integrated EDX system (Oxford Instrument/Aztec).

The presence of functional groups was investigated using a Fourier transform infrared spectrometer (FT-IR spectrometer, PerkinElmer Spectrum 100, USA) in ATR mode.

Tensile testing was performed using an Instron 5566 universal testing machine (Norwood, MA, USA) equipped with a 500 N load cell. The test pieces were 4 mm wide and clamped with a 40 mm span between the jaw faces, and a strain rate of 10% min^{-1} was used with a cross-head speed of 4 mm min^{-1}. The measurements were performed in a controlled environment at 50% relative humidity (RH) and 23 °C, where the papers were conditioned for about 24 h prior to the measurements. The grammage of the prepared sheets was determined gravimetrically on an analytical balance after conditioning the samples at 23 °C and 50% RH. Thickness was determined using a thickness gauge; six measuring points were employed on each sheet, and the sample thickness was used to convert the tensile strength from N m^{-1} to Pa. The density was calculated from the paper's grammage and thickness.

Electrical conductivity measurements of the PEDOT:PSS-adsorbed papers were conducted using a 2-point probe with a Source Meter 2401 (Keithley, Beaverton, USA). We measured the resistance R and estimated the conductivity.

Electrochemical measurements were performed using a potentiostat (Bio-Logic, Cromocol, Sweden). Cyclic voltammetry (CV) was carried out in a three-electrode configuration in 0.1 M NaCl aqueous electrolyte using an Ag/AgCl (3 M KCl) electrode as the reference electrode, a platinum wire as the counter electrode, and PEDOT:PSS-coated cellulose paper as the working electrode. CV measurements were recorded at scan rates ranging from 5 to 500 mV s^{-1} within a potential window of −0.8 to 0.8 V. For OECT gate characterization, CV was performed in a 0.5 M H_2SO_4 electrolyte over a voltage window of 0 to 1 V.

Electrochemical impedance spectroscopy measurements were conducted in a two-electrode, in-plane configuration using electrodes with the same dimensions as the OECT channel in 0.1 M NaCl aqueous electrolyte. An excitation amplitude of 10 mV was applied over a frequency range from 1 Hz to 1 MHz, with 50 points per decade.

4.8. OECT fabrication and characterization

Patterning of the papers was carried out using a CO_2 laser cutter (VSL 2.3, Universal Laser Inc.) with a vector design prepared in

Adobe Illustrator 2023. The patterned PEDOT:PSS paper comprised two contact pads and a single channel region (width ≈ 250 μm, length ≈ 5 mm), with the channel thickness varying from 45 to 65 μm depending on the PEDOT:PSS adsorption level and post-treatment conditions of the samples. Both contact pads were uniformly coated with conductive silver paint (Ladd Research) and dried overnight at room temperature.

A glass slide served as the substrate, pre-coated with transparent adhesive tape (Staples®) to enhance hydrophobicity. The patterned PEDOT:PSS paper was then attached to the substrate using two pieces of copper (Cu) tape (RS PRO Conductive Metallic Tape), with the contact pads sandwiched between the glass and the Cu tape. An insulating layer of nail lacquer was manually applied to define the channel area (width, $W = \sim 250$ μm; length, $L = \sim 2.5$ mm). The channel geometry and dimensions were identical for both the OECTs and the OECT-based hydrogen peroxide sensor. Initial characterization of the devices was performed in a 0.1 M NaCl aqueous electrolyte. Output characteristics of the initial electrical characterization of the OECTs were recorded by sweeping the drain voltage (V_d) from 0 V to −0.65 V in 0.05 V steps at successive gate voltages (V_g) ranging from −0.2 V to 0.8 V in 0.1 V increments. The transfer characteristics were obtained under a V_g sweep from −0.35 V to 0.8 V at a constant drain bias of −0.6 V. Stability characterization was performed under continuous ON/OFF operation for 1 h. Prior to data acquisition, the device was conditioned for 3 min under the same operating conditions. The drain current was then normalized to this initial value, and time-dependent measurements were conducted under repeated switching. The device was operated at a gate voltage of 0.8 V and a drain voltage of −0.6 V, with periodic switching between the ON and OFF states at approximately 4 s intervals. The drain current was continuously recorded throughout the measurement to assess device behavior under repeated switching conditions.

For electrical characterization of the OECTs, an Ag/AgCl gate electrode was used, whereas a gold gate electrode was employed for the sensor and subsequently modified as follows: gold electrodes were carefully cleaned using alumina polishing powders, followed by drop-casting of a PEDOT:PSS solution. The PEDOT:PSS formulation (containing 5% (v/v) ethylene glycol, 0.25% (v/v) DBSA, and 0.10% (v/v) GOPS) was filtered through a 0.45 μm polyethersulfone filter. A volume of 1 μL was drop-cast onto the rod electrode and annealed in an oven at 120 °C for 1 h. Platinum electrodeposition was subsequently performed on the PEDOT:PSS-coated gold electrodes. The gate electrode was functionalized with Pt nanoparticles *via* electrochemical deposition in an aqueous electrolyte comprising 5 mM H_2PtCl_6 and 50 mM H_2SO_4.[55] The gate served as the working electrode, and a potential sequence of 0.7 V for 10 s followed by −0.2 V for 15 s was applied using a (Bio-Logic, Cromocol, Sweden) potentiostat. Following electrodeposition, the electrodes were immersed in 0.5 M H_2SO_4, and cyclic voltammetry (CV) was conducted from −0.2 to 1.5 V for approximately 10 cycles at a scan rate of 20 and 100 mV s^{-1} as a control test to confirm successful Pt deposition prior to sensor measurements.

The sensor channel was stabilized by applying an initial 10 s holding step in the amperometric sequence, followed by stepwise operation with 60 s at $V_g = 0$ V and 60 s at $V_g = 0.8$ V for each hydrogen peroxide concentration. The sensor response was evaluated in 10 mM phosphate-buffered saline (PBS) across a hydrogen peroxide concentration range of 0.05–1000 μM. All the electrical characterization studies of the organic electrochemical transistors (OECTs) were carried out using two source-measure units (Keithley 4200A-SCS).

The LOD of the sensor was estimated using the 3σ criterion. Because the calibration curve follows a log–linear relationship, the detection limit was obtained by first determining the detection threshold in the signal domain and subsequently converting this value to concentration using the fitted calibration equation. The detection threshold was defined as:

$$y_{LOD} = y_{baseline} - 3\sigma \quad (2)$$

where $y_{baseline}$ represents the baseline signal and σ is the standard deviation of the baseline response. In the present dataset, replicate measurements at the lowest investigated concentration (0.05 μM) were used to estimate the baseline response and its standard deviation. The concentration corresponding to this threshold was obtained from the calibration equation by solving for concentration:

$$\log(C_{LOD}) = \frac{y_{LOD} - b}{a} \quad (3)$$

which yields

$$C_{LOD} = 10^{\frac{y_{LOD} - b}{a}} \quad (4)$$

Author contributions

The manuscript was written through contributions of all authors. All authors have given approval to the final version of the manuscript.

Conflicts of interest

There are no conflicts to declare.

Abbreviations

PEDOT:PSS	Poly(3,4-ethylenedioxythiophene):polystyrene sulfonate
CNF	Cellulose nanofibril
OECT	Organic electrochemical transistor
SEM	Scanning electron microscopy
EDX	Energy-dispersive X-ray spectroscopy
FT-IR	Fourier-transform infrared spectroscopy
DMSO	Dimethyl sulfoxide
IPA	Isopropyl alcohol
CV	Cyclic voltammetry
EIS	Electrochemical impedance spectroscopy
g_m	Transconductance

I_d	Drain current
V_g	Gate voltage
PBS	Phosphate-buffered saline;

Data availability

All data gathered to compile the paper's text and figures, including the supplementary information (SI), are readily available upon request. Supplementary information is available. See DOI: https://doi.org/10.1039/d6ta01756h.

Acknowledgements

We acknowledge the support from the Digital Cellulose Center and FibRe – Competence Centre for Design for Circularity: Lignocellulose-based thermoplastics, two centers within the Swedish Innovation Agency's competence center program (grant numbers 2022-03085 and 2019-00047, respectively), and the partners involved in these centers. E. Z. and M. M. gratefully acknowledge the Wallenberg Initiative Materials Science for Sustainability (WISE) funded by the Knut and Alice Wallenberg Foundation for support. E. Z. gratefully acknowledges the Swedish Research Council (Grant No. 2022-02855), and Formas – a Swedish Research Council for Sustainable Development (Grant No. 2022-00374) for support. This work was supported by AIMES – The center for integrated medical and engineering sciences (https://www.aimes.se), Karolinska Institutet (1-249/2019), KTH Royal Institute of Technology (VF-2019-0110), and Getinge AB (4.1599/2018).

References

1 A. Etale, A. J. Onyianta, S. R. Turner and S. J. Eichhorn, Cellulose: A Review of Water Interactions, Applications in Composites, and Water Treatment, *Chem. Rev.*, 2023, **123**(5), 2016–2048, DOI: 10.1021/ACS.CHEMREV.2C00477/ASSET/IMAGES/LARGE/CR2C00477_0024.JPEG.

2 C. Xiong, T. Wang, J. Han, Z. Zhang and Y. Ni, Recent Research Progress of Paper-Based Supercapacitors Based on Cellulose, *Energy Environ. Mater.*, 2024, **7**(3), e12651, DOI: 10.1002/EEM2.12651.

3 E. Jin, S. van Ewijk, K. S. Kanaoka, Y. A. Alamerew, H. Lin, Z. Cao, B. Jabarivelisdeh, K. F. Ehmann, M. R. Chertow and E. Masanet, Sustainability Assessment and Pathways for U.S. Domestic Paper Recycling, *Resour., Conserv. Recycl.*, 2023, **199**, 107249, DOI: 10.1016/J.RESCONREC.2023.107249.

4 S. Boufi, I. González, M. Delgado-Aguilar, Q. Tarrès, M. À. Pèlach and P. Mutjé, Nanofibrillated Cellulose as an Additive in Papermaking Process: A Review, *Carbohydr. Polym.*, 2016, **154**, 151–166, DOI: 10.1016/J.CARBPOL.2016.07.117.

5 E. Małachowska, M. Dubowik, A. Lipkiewicz, K. Przybysz and P. Przybysz, Analysis of Cellulose Pulp Characteristics and Processing Parameters for Efficient Paper Production, *Sustainability*, 2020, **12**(17), 7219, DOI: 10.3390/SU12177219.

6 F. Corcelli, G. Fiorentino, J. Vehmas and S. Ulgiati, Energy Efficiency and Environmental Assessment of Papermaking from Chemical Pulp - A Finland Case Study, *J. Cleaner Prod.*, 2018, **198**, 96–111, DOI: 10.1016/J.JCLEPRO.2018.07.018.

7 Y. Gao, Q. Li, Y. Shi and R. Cha, Preparation and Application of Cationic Modified Cellulose Fibrils as a Papermaking Additive, *Int. J. Polym. Sci.*, 2016, **2016**(1), 6978434, DOI: 10.1155/2016/6978434.

8 S. H. Osong, S. Norgren and P. Engstrand, Processing of Wood-Based Microfibrillated Cellulose and Nanofibrillated Cellulose, and Applications Relating to Papermaking: A Review, *Cellulose*, 2015, **23**(1), 93–123, DOI: 10.1007/S10570-015-0798-5.

9 R. Hollertz, L. Wågberg and C. Pitois, *Kraft-Pulp Based Material for Electrical Insulation. Proceedings of the Nordic Insulation Symposium*, 2015, No. 24, DOI: 10.5324/NORDIS.V0I24.2300.

10 Q. Luo, H. Shen, G. Zhou and X. Xu, A Mini-Review on the Dielectric Properties of Cellulose and Nanocellulose-Based Materials as Electronic Components, *Carbohydr. Polym.*, 2023, **303**, 120449, DOI: 10.1016/J.CARBPOL.2022.120449.

11 W. Ying, C. Zhou, H. Sun and W. Huang, Paper-Based Flexible Electronic Devices: Processing, Integration, and Applications, *npj Flexible Electron.*, 2025, **9**(1), 1–30, DOI: 10.1038/S41528-025-00446-Z.

12 X. Wang and C. Yu, Flexible Low-Voltage Paper Transistors Harnessing Ion Gel/Cellulose Fiber Composites, *J. Mater. Res.*, 2020, **35**(8), 940–948, DOI: 10.1557/JMR.2019.303/FIGURES/6.

13 E. J. Strand, A. Gopalakrishnan, C. A. Crichton, M. J. Palizzi, O. Lee, T. Borsa, E. Bihar, P. Goodrich, A. C. Arias, S. E. Shaheen, R. R. McLeod and G. L. Whiting, Ultrathin Screen-Printed Plant Wearable Capacitive Sensors for Environmental Monitoring, *Adv. Sens. Res.*, 2025, **4**(3), 2400177, DOI: 10.1002/ADSR.202400177.

14 Q. T. Lai, H. Q. Liang, X. G. Tang, D. Zhang, V. A. L. Roy and Q. J. Sun, Printing Paper-Derived Ultralight and Highly Sensitive E-Skin for Health Monitoring and Information Encryption, *J. Alloys Compd.*, 2024, **976**, 173411, DOI: 10.1016/J.JALLCOM.2023.173411.

15 N. Kumar, S. Y. Lee and S. J. Park, Recent Progress and Challenges in Paper-Based Microsupercapacitors for Flexible Electronics: A Comprehensive Review, *ACS Appl. Mater. Interfaces*, 2024, **16**(17), 21367–21382, DOI: 10.1021/ACSAMI.4C01438.

16 H. Yang, H. Zheng, Y. Duan, T. Xu, H. Xie, H. Du and C. Si, Nanocellulose-Graphene Composites: Preparation and Applications in Flexible Electronics, *Int. J. Biol. Macromol.*, 2023, **253**, 126903, DOI: 10.1016/J.IJBIOMAC.2023.126903.

17 M. M. Hamedi, A. Hajian, A. B. Fall, K. Hkansson, M. Salajkova, F. Lundell, L. Wgberg and L. A. Berglund, Highly Conducting, Strong Nanocomposites Based on Nanocellulose-Assisted Aqueous Dispersions of Single-Wall Carbon Nanotubes, *ACS Nano*, 2014, **8**(3), 2467–2476, DOI: 10.1021/NN4060368/SUPPL_FILE/NN4060368_SI_001.PDF.

18 T. Benselfelt, J. Shakya, P. Rothemund, S. B. Lindström, A. Piper, T. E. Winkler, A. Hajian, L. Wågberg, C. Keplinger and M. M. Hamedi, Electrochemically Controlled Hydrogels with Electrotunable Permeability and Uniaxial Actuation, *Adv. Mater.*, 2023, **35**(45), 2303255, DOI: 10.1002/ADMA.202303255.

19 L. Li, W. Tian, A. Vahidmohammadi, J. Rostami, B. Chen, K. Matthews, F. Ram, T. Pettersson, L. Wågberg, T. Benselfelt, Y. Gogotsi, L. A. Berglund, M. M. Hamedi, L. Li, W. Tian, J. Rostami, B. Chen, F. Ram, T. Pettersson, L. Wågberg, T. Benselfelt, L. A. Berglund, M. M. Hamedi, A. Vahidmohammadi, K. Matthews and Y. Gogotsi, Ultrastrong Ionotronic Films Showing Electrochemical Osmotic Actuation, *Adv. Mater.*, 2023, **35**(45), 2301163, DOI: 10.1002/ADMA.202301163.

20 Y. C. Gorur, P. A. Larsson and L. Wågberg, Self-Fibrillating Cellulose Fibers: Rapid in Situ Nanofibrillation to Prepare Strong, Transparent, and Gas Barrier Nanopapers, *Biomacromolecules*, 2020, **21**(4), 1480–1488, DOI: 10.1021/ACS.BIOMAC.0C00040/SUPPL_FILE/BM0C00040_LIVESLIDES.MP4.

21 A. Hajian, K. Jain, N. I. Kilic, A. Iakunkov, C. M. Subramaniyam, L. Wågberg, P. A. Larsson and M. M. Hamedi, Recyclable Electroactive Paper Based on Cationic Fibers Adaptable to Industrial Papermaking, *Cellulose*, 2024, **31**(14), 8837–8849, DOI: 10.1007/S10570-024-06128-9/FIGURES/3.

22 J. Sjölund, G. Westman, L. Wågberg and P. A. Larsson, On the Determination of Charge and Nitrogen Content in Cellulose Fibres Modified to Contain Quaternary Amine Functionality, *Carbohydr. Polym.*, 2025, **347**, 122734, DOI: 10.1016/J.CARBPOL.2024.122734.

23 A. Sjöstedt, J. Wohlert, P. T. Larsson and L. Wågberg, Structural Changes during Swelling of Highly Charged Cellulose Fibres, *Cellulose*, 2015, **22**(5), 2943–2953, DOI: 10.1007/S10570-015-0701-4.

24 S. Chen, L. Liang, Y. Zhang, K. Lin, M. Yang, L. Zhu, X. Yang, L. Zang and B. Lu, PEDOT:PSS-Based Electronic Materials: Preparation, Performance Tuning, Processing, Applications, and Future Prospect, *Prog. Polym. Sci.*, 2025, **166**, 101990, DOI: 10.1016/J.PROGPOLYMSCI.2025.101990.

25 K. Jain, A. Y. Mehandzhiyski, I. Zozoulenko and L. Wågberg, PEDOT:PSS Nano-Particles in Aqueous Media: A Comparative Experimental and Molecular Dynamics Study of Particle Size, Morphology and z-Potential, *J. Colloid Interface Sci.*, 2021, **584**, 57–66, DOI: 10.1016/J.JCIS.2020.09.070.

26 N. Inci Kilic, K. Matthews, G. Marco Saladino, Y. Gogotsi, P. A. Larsson, M. Max Hamedi, N. I. Kilic, P. A. Larsson, M. M. Hamedi, K. Matthews, Y. A. Gogotsi and G. M. Saladino, 3D-Printed Crosslinked Nanocellulose-MXene Hydrogels and Aerogels with High Strength and Conductivity, *Small*, 2025, e07491, DOI: 10.1002/SMLL.202507491.

27 E. Sjostrom, The Origin of Charge on Cellulosic Fibers, *Nord. Pulp Pap. Res. J.*, 1989, **4**(2), 90–93, DOI: 10.3183/NPPRJ-1989-04-02-P090-093.

28 P. T. Larsson, A. Svensson and L. Wågberg, A New, Robust Method for Measuring Average Fibre Wall Pore Sizes in Cellulose I Rich Plant Fibre Walls, *Cellulose*, 2013, **20**(2), 623–631, DOI: 10.1007/S10570-012-9850-X.

29 C. Fu, C. Lin, W. Zhang, Y. Lin, J. Xiu, Y. Ni and L. Huang, Preparation of Micro-Fibrillated Cellulose Fibers by a Simple Two-Step Refining Process for Paper- Based Flexible Electronic Devices, *Chem. Eng. J.*, 2023, **468**, 143516, DOI: 10.1016/J.CEJ.2023.143516.

30 H. Chen, A. Park, J. A. Heitmann and M. A. Hubbe, Importance of Cellulosic Fines Relative to the Dewatering Rates of Fiber Suspensions, *Ind. Eng. Chem. Res.*, 2009, **48**(20), 9106–9112, DOI: 10.1021/IE9006613/ASSET/IMAGES/LARGE/IE-2009-006613_0001.JPEG.

31 J. Sjölund, G. Westman, L. Wågberg and P. A. Larsson, High-Consistency Modification of Cellulose Fibers: Resource-Efficient Introduction of Cationic Charges, and Their Effect on Fiber and Nanofibril Properties, *Carbohydr. Polym.*, 2025, **352**, 123254, DOI: 10.1016/J.CARBPOL.2025.123254.

32 W. Wu, H. Zeng, Y. Li, H. Jiang, J. Wu, Z. Li, W. Zhang, X. Wang and Q. Xue, Structural-Induced Effects of DES in PEDOT:PSS Aqueous Polymerization, *Polym. Test.*, 2023, **129**, 108272, DOI: 10.1016/J.POLYMERTESTING.2023.108272.

33 G. Hassan, M. Sajid and C. Choi, Highly Sensitive and Full Range Detectable Humidity Sensor Using PEDOT:PSS, Methyl Red and Graphene Oxide Materials, *Sci. Rep.*, 2019, **9**(1), 1–10, DOI: 10.1038/s41598-019-51712-w.

34 P. Li, K. Sun and J. Ouyang, Stretchable and Conductive Polymer Films Prepared by Solution Blending, *ACS Appl. Mater. Interfaces*, 2015, **7**(33), 18415–18423, DOI: 10.1021/ACSAMI.5B04492/ASSET/IMAGES/LARGE/AM-2015-04492K_0012.

35 E. Hosseini, V. Ozhukil Kollath and K. Karan, The Key Mechanism of Conductivity in PEDOT:PSS Thin Films Exposed by Anomalous Conduction Behaviour upon Solvent-Doping and Sulfuric Acid Post-Treatment, *J. Mater. Chem. C*, 2020, **8**(12), 3982–3990, DOI: 10.1039/C9TC06311K.

36 D. J. Yun, H. Ra, J. M. Kim, J. H. Lee, S. H. Park, J. Hwang, J. G. Chung, S. H. Kim, Y. S. Kim, Y. J. Jeong and S. H. Lee, A Study on Distinctive Transition Mechanism of Sulfuric Acid Treatment on Performance Enhancement of Poly(3,4-Ethylenedioxythiophene): Polystyrene Based Electrodes Depending on Multiwall Carbon Nanotube Dose, *Appl. Surf. Sci.*, 2019, **487**, 480–487, DOI: 10.1016/J.APSUSC.2019.05.125.

37 S. Liu, H. Deng, Y. Zhao, S. Ren and Q. Fu, The Optimization of Thermoelectric Properties in a PEDOT:PSS Thin Film through Post-Treatment, *RSC Adv.*, 2014, **5**(3), 1910–1917, DOI: 10.1039/C4RA09147G.

38 S. Wu, S. Shi, R. Liu, C. Wang, J. Li and L. Han, The Transformations of Cellulose after Concentrated Sulfuric Acid Treatment and Its Impact on the Enzymatic Saccharification, *Biotechnol. Biofuels Bioprod.*, 2023, **16**(1), 36, DOI: 10.1186/s13068-023-02293-4.

39 M. Borrega, P. Ahvenainen and E. Kontturi, Impact of Hydrothermal and Alkaline Treatments of Birch Kraft Pulp

on the Levelling-off Degree of Polymerization (LODP) of Cellulose Microfibrils, *Cellulose*, 2018, **25**(11), 6811–6818, DOI: 10.1007/s10570-018-2017-7.

40 X. Chen, F. Jiang, Q. Jiang, Y. Jia, C. Liu, G. Liu, J. Xu, X. Duan, C. Zhu, G. Nie and P. Liu, Conductive and Flexible PEDOT-Decorated Paper as High Performance Electrode Fabricated by Vapor Phase Polymerization for Supercapacitor, *Colloids Surf., A*, 2020, **603**, 125173, DOI: 10.1016/J.COLSURFA.2020.125173.

41 P. Isacsson, K. Jain, A. Fall, V. Chauve, A. Hajian, H. Granberg, L. Boiron, M. Berggren, K. Håkansson, J. Edberg, I. Engquist and L. Wågberg, Production of Energy-Storage Paper Electrodes Using a Pilot-Scale Paper Machine, *J. Mater. Chem. A*, 2022, **10**(40), 21579–21589, DOI: 10.1039/D2TA04431E.

42 H. Du, M. Zhang, K. Liu, M. Parit, Z. Jiang, X. Zhang, B. Li and C. Si, Conductive PEDOT:PSS/Cellulose Nanofibril Paper Electrodes for Flexible Supercapacitors with Superior Areal Capacitance and Cycling Stability, *Chem. Eng. J.*, 2022, **428**, 131994, DOI: 10.1016/J.CEJ.2021.131994.

43 H. Wang, U. Ail, R. Gabrielsson, M. Berggren and X. Crispin, Ionic Seebeck Effect in Conducting Polymers, *Adv. Energy Mater.*, 2015, **5**(11), 1500044, DOI: 10.1002/AENM.201500044.

44 R. Del Olmo, M. Forsyth and N. Casado, Mixed Ionic-Electronic Conductors Based on Polymer Composites, *Eng. Mater.*, 2022, 493–532, DOI: 10.1007/978-3-030-94319-6_17.

45 R. A. Huggins, Simple Method to Determine Electronic and Ionic Components of the Conductivity in Mixed Conductors a Review, *Ionics*, 2002, **8**(3), 300–313, DOI: 10.1007/BF02376083.

46 Y. Ko, J. Kim, D. Kim, G. Kwon, Y. Yamauchi and J. You, Fabrication of Highly Conductive Porous Cellulose/PEDOT:PSS Nanocomposite Paper via Post-Treatment, *Nanomaterials*, 2019, **9**(4), 612, DOI: 10.3390/NANO9040612.

47 F. Hik, E. Taatizadeh, S. E. Takalloo and J. D. W. Madden, Fast Electrochemical Response of PEDOT:PSS Electrodes through Large Combined Increases to Ionic and Electronic Conductivities, *Electrochim. Acta*, 2023, **468**, 143136, DOI: 10.1016/J.ELECTACTA.2023.143136.

48 H. S. Park, S. J. Ko, J. S. Park, J. Y. Kim and H. K. Song, Redox-Active Charge Carriers of Conducting Polymers as a Tuner of Conductivity and Its Potential Window, *Sci. Rep.*, 2013, **3**(1), 2454, DOI: 10.1038/srep02454.

49 D. A. Bernards and G. G. Malliaras, Steady-State and Transient Behavior of Organic Electrochemical Transistors, *Adv. Funct. Mater.*, 2007, **17**(17), 3538–3544, DOI: 10.1002/ADFM.200601239.

50 X. Wu, M. Stephen, T. C. Hidalgo, T. Salim, J. Surgailis, A. Surendran, X. Su, T. Li, S. Inal and W. L. Leong, Ionic-Liquid Induced Morphology Tuning of PEDOT:PSS for High-Performance Organic Electrochemical Transistors, *Adv. Funct. Mater.*, 2022, **32**(1), 2108510, DOI: 10.1002/ADFM.202108510.

51 D. Khodagholy, J. Rivnay, M. Sessolo, M. Gurfinkel, P. Leleux, L. H. Jimison, E. Stavrinidou, T. Herve, S. Sanaur, R. M. Owens and G. G. Malliaras, High Transconductance Organic Electrochemical Transistors, *Nat. Commun.*, 2013, **4**(1), 2133, DOI: 10.1038/ncomms3133.

52 Y. J. Jo, S. Y. Kim, J. H. Hyun, B. Park, S. Choy, G. R. Koirala and T. il Kim, Fibrillary Gelation and Dedoping of PEDOT:PSS Fibers for Interdigitated Organic Electrochemical Transistors and Circuits, *npj Flexible Electron.*, 2022, **6**(1), 1–11, DOI: 10.1038/S41528-022-00167-7.

53 J. T. Friedlein, R. R. McLeod and J. Rivnay, Device Physics of Organic Electrochemical Transistors, *Org. Electron.*, 2018, **63**, 398–414, DOI: 10.1016/J.ORGEL.2018.09.010.

54 Z. Wang, W. Gao, X. Niu, Y. Liu, Z. Jin, F. Zhang, Z. Cheng, X. Jiang, W. Zhang, T. Wang, J. Ji, X. Chai and S. Sang, Ultra-Low LOD H2O2 Sensor Based on Synergistic Nernst Potential Effect, *Adv. Sci.*, 2025, **12**(26), 2413898, DOI: 10.1002/ADVS.202413898;.

55 A. Enrico, S. Buchmann, F. De Ferrari, Y. Lin, Y. Wang, W. Yue, G. Mårtensson, G. Stemme, M. M. Hamedi, F. Niklaus, A. Herland and E. Zeglio, Cleanroom-Free Direct Laser Micropatterning of Polymers for Organic Electrochemical Transistors in Logic Circuits and Glucose Biosensors, *Adv. Sci.*, 2024, **11**(27), 2307042, DOI: 10.1002/ADVS.202307042;ISSUE:ISSUE.

56 C. Diacci, T. Abedi, J. W. Lee, E. O. Gabrielsson, M. Berggren, D. T. Simon, T. Niittylä and E. Stavrinidou, Diurnal in Vivo Xylem Sap Glucose and Sucrose Monitoring Using Implantable Organic Electrochemical Transistor Sensors, *iScience*, 2021, **24**(1), 101966, DOI: 10.1016/J.ISCI.2020.101966.

57 J. E. Giaretta, H. Duan, F. Oveissi, S. Farajikhah, F. Dehghani and S. Naficy, Flexible Sensors for Hydrogen Peroxide Detection: A Critical Review, *ACS Appl. Mater. Interfaces*, 2022, **14**(18), 20491–20505, DOI: 10.1021/ACSAMI.1C24727.

58 A. A. Andreo Acosta, P. Blondeau and F. J. Andrade, Compact Paper-Based Quasi-Solid-State Organic Electrochemical Transistor (QSS-OECT) for Sensing Hydrogen Peroxide, *ACS Appl. Electron. Mater.*, 2025, **7**(15), 6791–6799, DOI: 10.1021/ACSAELM.5C00559.

59 Y. Song, S. Xu and O. Parlak, Bilirubin Sensing Using Organic Electrochemical Transistors: Role of Gate Materials and Operational Parameters, *Adv. Healthcare Mater.*, 2025, e02481, DOI: 10.1002/ADHM.202502481.

60 N. Fumeaux, C. P. Almeida, S. Demuru and D. Briand, Organic Electrochemical Transistors Printed from Degradable Materials as Disposable Biochemical Sensors, *Sci. Rep.*, 2023, **13**(1), 11467, DOI: 10.1038/s41598-023-38308-1.

61 W. Luo, M. E. Abbas, L. Zhu, K. Deng and H. Tang, Rapid Quantitative Determination of Hydrogen Peroxide by Oxidation Decolorization of Methyl Orange Using a Fenton Reaction System, *Anal. Chim. Acta*, 2008, **629**(1–2), 1–5, DOI: 10.1016/j.aca.2008.09.009.